ACS APPLIED MATERIALS & INTERFACES

Research Article

www.acsami.org

# Fabrication of Highly Sensitive and Stable Hydroxylamine Electrochemical Sensor Based on Gold Nanoparticles and Metal−Metalloporphyrin Framework Modified Electrode

Yang Wang,*[,†,‡] Lu Wang,[†] Huanhuan Chen,[†] Xiaoya Hu,[†] and Shengqian Ma*[,‡]

[†]School of Chemistry and Chemical Engineering, Yangzhou University, Yangzhou 225002, PR China

[‡]Department of Chemistry, University of South Florida, 4202 East Fowler Avenue, Tampa, Florida 33620, United States

**ABSTRACT:** This paper describes the immobilization of gold nanoparticles on metal−metalloporphyrin frameworks (AuNPs/MMPF-6(Fe)) through electrostatic adsorption. The composites were characterized by powder X-ray diffraction, zeta potential, transmission electron microscopy, electrochemical impedance spectroscopy, and voltammetric methods. MMPF-6(Fe) exhibited a pair of redox peaks of the Fe(III)TCPP/Fe(II)TCPP redox couple. The AuNPs/MMPF-6(Fe)-based electrochemical sensor demonstrates a distinctly higher electrocatalytic response to the oxidation of hydroxylamine due to the synergic effect of the gold metal nanoparticles and metal−metalloporphyrin matrix. The voltammetric current response exhibits two linear dynamic ranges, 0.01−1.0 and 1.0−20.0 $\mu$mol $L^{-1}$, and the detection limit was as low as 0.004 $\mu$mol $L^{-1}$ (S/N = 3). Moreover, the biosensor exhibits high reproducibility and stability in acid solution. Our work not only offers a simple way to achieve the direct electrochemical behavior of metalloporphyrin but also expands the potential applications of MOFs-based composites in bioanalysis.

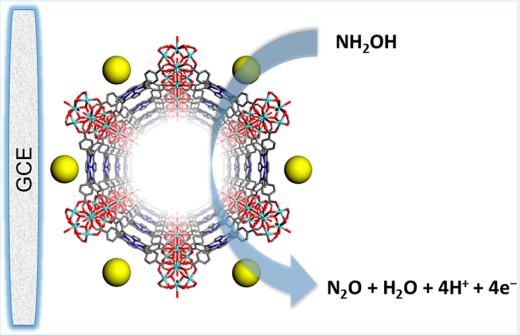


**KEYWORDS:** *metal−organic framework, metal−metalloporphyrin frameworks, gold nanoparticles, electrochemical sensor, hydroxylamine*

## INTRODUCTION

Hydroxylamine, an oxygenated derivative of ammonia, is commonly used as a raw material in industrial and pharmaceutical processes.[1,2] However, it is also well-known to be moderately toxic to animals, plants, and humans, which can produce both reversible and irreversible physiological changes.[3] Relatively little information is available as to the acute toxicity of hydroxylamine, and the oral $LD_{50}$ of hydroxylamine hydrochloride for the mouse was reported as 420 versus 400 mg/kg by two different sources.[4] It has been reported that hydroxylamine at millimolar levels can remain stable for several hours (pH 4.0) but for only 1 h in the presence of air (pH 7.8).[5,6] Hence, the direct detection of hydroxylamine is difficult in environmental and biologic samples due to the lower concentration and instability.[7] Many methods have been developed to detect hydroxylamine over the past decade. Among these, an electrochemical method possesses many advantages, such as good selectivity, fast detection, high sensitivity, and low cost.[8−10] These features have spurred enormous research in electrochemical biosensor/sensors for hydroxylamine detection.[11−15]

Metal−organic frameworks (MOFs) represent an intriguing class of highly porous materials consisting of metal ions and organic ligands.[16,17] Currently, significant progress has been made in the application of synthesizing new MOFs and investigating their applications in catalysis and gas adsorption/separation.[18−20] However, because of the poor conductivity of MOFs at the conventional electrode surface as well as the instability of MOFs structures in aqueous solutions, the fabrication of MOFs-based composites for electrochemical sensor application remains a challenge.[21−23] To extend the scope of applications of MOFs, many conductive materials (graphene oxide and macroporous carbon) were combined with MOFs to construct novel electrochemical sensor to improve their electrochemical performance.[24,25]

Because of excellent catalytic activity and hospitable environment for biomolecules, gold nanoparticles (AuNPs) are increasingly used in numerous electrochemical fields.[26,27] The good conductivity of AuNPs can improve the electron transfer and amplify the electrochemical signal. Meanwhile, the encapsulation of AuNPs inside the MOFs has been reported and exhibits high catalytic activity in heterogeneous catalysis.[28−31] However, the high catalytic effect of the AuNPs inside the MOFs was almost completely suppressed when they were used as electrode materials in our present studies.

Given the complementary characteristics of AuNPs and MOFs, herein we develop an alternative approach of constructing AuNPs/metal−metalloporphyrin composites.

**Received:** April 22, 2016
**Accepted:** June 28, 2016
**Published:** June 28, 2016





DOI: 10.1021/acsami.6b04819
*ACS Appl. Mater. Interfaces* 2016, 8, 18173−18181

The metal−metalloporphyrin framework, MMPF-6(Fe) ($Zr_6O_8(H_2O)_8(TCPP{\cdot}FeCl)_2$), was selected as a representative MOF support because it has large pore size, high surface area, good chemical stability to water and organic media, and biomimetic catalytic activities.[32] The characterization of the resulting material indicated that AuNPs were not entered into the host matrix but rather well-dispersed on the outer surface of metal−metalloporphyrin crystals. The combination of conducting gold nanoparticles and MMPF-6(Fe) can provide potential electrochemical candidates for biochemical sensor due to the strong catalysis sites, enlarged active surface area, and their high conductivity. The established method was employed for ultrasensitive hydroxylamine determination in real pharmaceutical and water samples.

## EXPERIMENTAL SECTION

**Reagents and Materials.** Hydroxylamine stock solution (0.01 mol $L^{-1}$) was obtained by dissolving 0.66 mL of 50% hydroxylamine aqueous solution (Jinshan Chemicals, Shanghai, China) in 100 mL deionized water. Phosphate-buffered solution (PBS, 0.1 mol $L^{-1}$, pH 7.0) was prepared by using $Na_2HPO_4$ and $NaH_2PO_4$. Hydrogen tetrachloroaurate trihydrate ($HAuCl_4{\cdot}3H_2O$), trisodium citrate, zirconyl chloride octahydrate, pyrrole, methyl *p*-formylbenzoate, formic acid, *N*,*N*-dimethylformamide (DMF), hydrochloric acid, potassium hydroxide, tetrahydrofuran, methyl alcohol, acetone, trichloromethane, propionic acid, ferrous chloride tetrahydrate, and anhydrous magnesium sulfate were of analytical grade. Environmental water samples were obtained from the lab and local river, respectively. The oxyurea capsule and pyridine-2-aldoxime methyl iodide (PAM injection) were purchased from local drugstore. Tetrakis(4-carboxyphenyl)-porphyrin ($H_2TCPP$) and Fe(III)-tetra(4-carboxyphenyl)-porphyrin chloride (Fe-TCPP) ligands were prepared based on previous reports.[33,34]

**Instrumentation.** Electrochemical measurements and impedance spectroscopy were carried out with CHI852C electrochemical analyzer (Shanghai Chenhua Co., China). A traditional three-electrode system was employed in the measurements, with an AuNPs/MMPF-6(Fe)-modified glassy carbon electrode (GCE) as the working electrode, an Ag/AgCl electrode as the reference electrode and a platinum wire as the auxiliary electrode. Zeta potential was measured with Zetasizer Nano ZSP (Malvern, England). The powder X-ray diffraction (XRD) analyses were carried out by using a D8 Advance X-ray diffractometer (Bruker Co., Germany) from 2.5 to 50°. The transmission electron micrograph (TEM) images were obtained with the Tecnai 12 (Holland Philips).

**Synthesis of MMPF-6 and MMPF-6(Fe).** MMPF-6 and MMPF-6(Fe) were synthesized according to the previous literature.[32] Briefly, zirconyl chloride octahydrate (37.5 mg), $H_2TCPP$ (6.5 mg) or Fe-TCPP (6.5 mg), and formic acid (7 mL) were ultrasonically dissolved in DMF (10 mL). After heating at 130 °C for 72 h, the single crystals were collected by filtration and washed with DMF (5 × 10 mL) over a 3 h period and acetone (5 × 30 mL) over a 5 day period, respectively. Finally, the acetone was removed by heating at 120 °C for 48 h.

**Synthesis of AuNPs.** AuNPs were synthesized by a citrate reduction of $HAuCl_4$.[35] Distilled water containing $HAuCl_4$ solution (200 mL, 0.05% by weight) was refluxed during stirring. When the $HAuCl_4$ solution started to boil, 5 mL of trisodium citrate (1% by weight) was added rapidly, and the reaction was continued until the color turned dark red. After reaction, the mixture was cooled to room temperature under stirring conditions and was then stored at 4 °C for further use.

**Preparation of AuNPs/MMPF-6(Fe)/GCE.** The bare GCE was first polished with alumina slurry, followed by rinsing ultrasonically with anhydrous alcohol and distilled deionized water, and finally allowed to dry in $N_2$ blowing. MMPF-6(Fe) (1.0 mg) was dissolved in 1.0 mL of DMF by sonication to form a homogeneously suspension. Then, 5 μL of the MMPF-6(Fe) suspension was dropped on the fresh pretreated GCE surface to obtain MMPF-6(Fe)/GCE. The immobilization of AuNPs on the MMPF-6(Fe)-modified electrode was achieved by immersing the MMPF-6(Fe)-modified electrode into the colloidal AuNPs solution for 10 min and dried in the air.

**Sample Pretreatment.** Oxyurea capsule powder (0.0025 g) was dissolved in 7 mol $L^{-1}$ HCl solution for digestion. After cooling to room temperature, the mixture was neutralized with sodium hydroxide and transferred to a 20 mL calibrated flask with deionized water. As for PAM injection, PAM injection (12.0 mL) was pretreated by applying above procedure. The environmental water samples were filtered using a 0.45 μm membrane filter to eliminate suspended particles and analyzed without delay.

## RESULTS AND DISCUSSION

**Characterization of AuNPs/MMPF-6(Fe).** In the present work, MMPF-6(Fe) was prepared hydrothermally, as described in the Experimental Section. To form a robust homogeneous film on the electrode surface, MMPF-6(Fe) was pretreated by grinding and ultrasonication before use. The powder scraped from the electrode was confirmed by comparing the XRD patterns of the powder and the simulated diffraction patterns (Figure 1a). The well-tallied patterns indicate that MMPF-6(Fe) with high quality was successfully prepared and the structure was preserved after pretreatment.[32−35] The BET surface area of MMPF-6(Fe) is 2101 $m^2\ g^{-1}$, and the pore sizes of MMPF-6 (Fe) by pore size distribution analysis are about 10 and 33 Å. The zeta potential value of MMPF-6(Fe) decreases with the increase of solution pH, and the isoelectrical point is calculated to be 7.4 (Figure 1b). Figure 1c shows that the monodisperse gold nanoparticles are spherical in shape, with a mean diameter of 15.28 ± 0.5 nm. AuNPs/MMPF-6(Fe) was obtained by immersing the MOFs-modified electrode in AuNPs solution for 10 min, and the obtained materials were scraped off from the electrode for the subsequent TEM analysis. As shown in Figure 1d, MMPF-6(Fe) did not show perfect crystallinity of the as-synthesized needle shape after pretreatment. Au nanoparticles are mainly dispersed on external surface, and no obvious aggregation was observed. The BET surface area (2058 $m^2$) and total pore size (10 and 33 Å) of AuNPs/MMPF-6(Fe) were nearly unchanged compared with MMPF-6(Fe). The thickness of the coated AuNPs/MMPF-6(Fe) layer

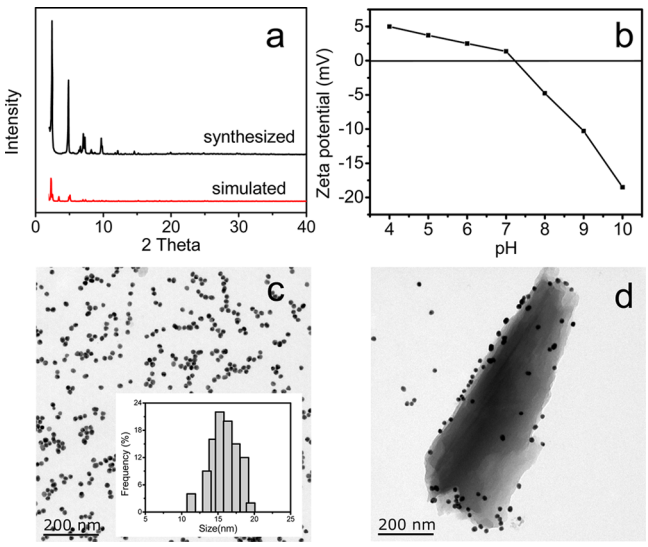


**Figure 1.** X-ray diffraction pattern (a) and zeta potential value (b) of MMPF-6(Fe). TEM images of AuNPs (c) and AuNPs/MMPF-6(Fe) (d). Inset shows the histogram of AuNPs distribution.


DOI: 10.1021/acsami.6b04819
ACS Appl. Mater. Interfaces 2016, 8, 18173−18181

was measured to be about 10 $\mu$m (determinated by confocal laser scanning microscopy). The MMPF-6(Fe) has positive charge in trisodium citrate solution (pH 6.0), and the AuNPs layer is formed due to the electrostatic interactions because the AuNPs are negatively charged in citrate solution.

Electrochemical impedance spectra of $[Fe(CN)_6]^{3-/4-}$ is usually employed to investigate the interfacial electron transfer properties of different electrodes. Figure 2 shows the

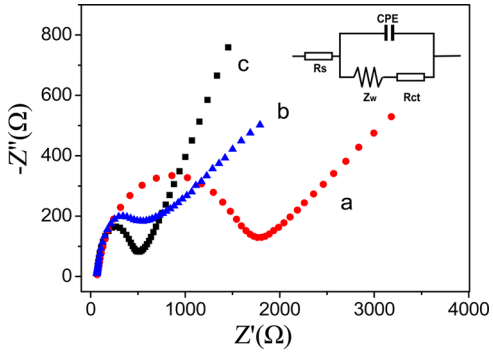


**Figure 2.** Electrochemical impedance spectra of the bare GCE (a), MMPF-6(Fe)/GCE (b), and AuNPs/MMPF-6(Fe)/GCE (c) in 0.1 mol $L^{-1}$ KCl solution containing 5 mmol $L^{-1}$ $Fe(CN)_6^{3-/4-}$.

electrochemical impedance spectra of bare GCE, MMPF-6(Fe)/GCE, and AuNPs/MMPF-6(Fe)/GCE, Figure 2a–c, respectively. For bare GCE, the electron transfer resistance value was 1470 Ω. At MMPF-6(Fe)/GCE, the value of resistance was changed to 745 Ω, suggesting that the bare GCE was coated efficiently by MMPF-6(Fe). A distinct decrease in the interfacial electron transfer resistance was also seen when AuNPs were dispersed on the out surface of MOFs (403 Ω). There is no doubt that AuNPs could improve the conductivity of the MOFs and facilitated the electron transfer between solution and electrode interface. This result also indicated that AuNPs/MMPF-6(Fe)/GCE was successfully fabricated. The amount of AuNPs has an important role in the voltammetric behavior of hydroxylamine. Hence, the effect of immersion time (10, 20, 30, and 40 min) on the peak currents of hydroxylamine was explored. The peak current intensity increased slightly with immersion time increasing up to 30 min. With further increase of the immersion time, the current intensity nearly remains the same. This means that a saturated immobilization of AuNPs on MMPF-6(Fe) was achieved. In this paper, to decrease the electrode preparation time and increase the sample frequency, a 10 min immersion time was selected in the subsequent experiments.

**Electrochemical Behavior of AuNPs/MMPF-6(Fe)/GCE.** As shown in Figure 3, the cyclic voltammograms of bare GCE did not display any redox peak (curve a), whereas GCEs modified with MMPF-6(Fe) showed a pair of observable peaks at −0.1 and −0.3 V (curve b). These peaks were be assigned to the redox couple of Fe(III)TCPP/Fe(II)TCPP in MMPF-6(Fe).[36] It was observed that with an increase of pH from 5 to 9, the oxidation potential of the MMPF-6(Fe)/GCE was shifted toward less positive values and showed a linear relationship with a slope of −62.0 mV $pH^{-1}$. This slope was very close to the anticipated Nerstian value of −59.1 mV $pH^{-1}$, thus meaning that the same number of electrons and protons are transferred in the electrode oxidation reaction. The AuNPs/MMPF-6(Fe)/GCE displayed a couple of redox peaks, and the

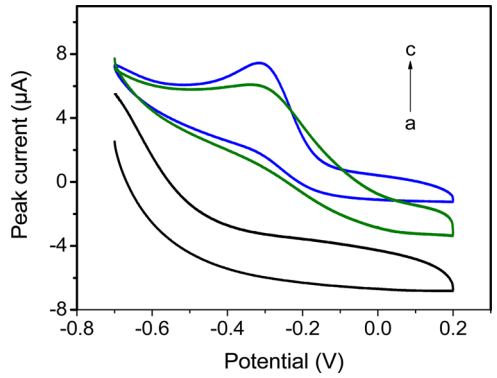


**Figure 3.** Cyclic voltammograms of a bare GCE (a), MMPF-6(Fe)/GCE (b), and AuNPs/MMPF-6(Fe)/GCE (c) in 0.1 mol $L^{-1}$ PBS (pH 7.0) at 100 mV $s^{-1}$.

anodic peak current was 5.17 $\mu$A, which is 1.78 times higher than that of the MMPF-6(Fe)-modified GCE (2.90 $\mu$A), further confirming the effect of AuNPs in accelerating the electron transfer rate between MMPF-6(Fe) and the GCE.

**Cyclic Voltammetric Behaviors of Hydroxylamine.** The cyclic voltammograms at bare GCE, AuNPs/GCE, MMPF-6(Fe)/GCE, and AuNPs/MMPF-6(Fe)/GCE were recorded and shown in Figure 4a–d, respectively. The oxidation peaks of

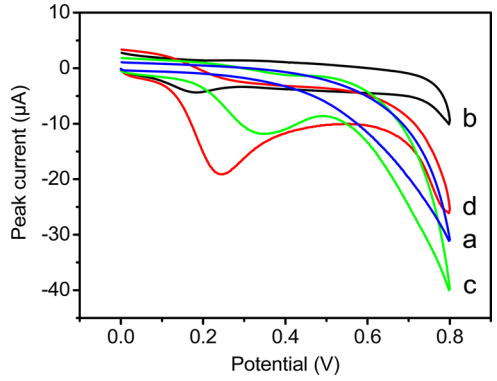


**Figure 4.** Cyclic voltammograms of 0.20 mmol $L^{-1}$ hydroxylamine at the bare GCE (a) and GCEs modified with AuNPs (b), MMPF-6(Fe) (c), and AuNPs/MMPF-6(Fe)/GCE (d) in 0.1 mol $L^{-1}$ PBS (pH 7.0).

hydroxylamine at these electrodes were completely irreversible. No oxidation peak was observed at the bare GCE, whereas AuNPs/GCE gave a signal at 0.2 V, indicating that AuNPs had clearly catalytic effect activity to the electro-oxidation of hydroxylamine. Compared with those of the bare GCE and AuNPs/GCE, a high and broad current signal was obtained after MMPF-6(Fe) was immobilized on GCE surface, although the cyclic voltammogram obtained at MMPF-6(Fe)/GCE presented a larger overpotential at about 0.35 V (Figure 4c). These could occur in two ways: (1) The relative large surface area of the MMPF-6(Fe)/GCE can offer more electrochemical active sites and improves the electrochemical response. (2) Hydroxylamine molecules can penetrate into the MMPF-6(Fe) channel, and the size and shape of the pores structure result in size- and shape-selectivity over the guests that were accumulated on the electrode surface. Another control experiment was added with Fe(III)-porphyrin/GCE for hydroxylamine oxidation with the same Fe(III) content. The


DOI: 10.1021/acsami.6b04819
ACS Appl. Mater. Interfaces 2016, 8, 18173−18181

current intensity at the MMPF-6(Fe)/GCE was improved in contrast to that at the Fe(III)-porphyrins/GCE, which also demonstrated the structural feature of the MMPF-6(Fe), was favorable for electrocatalytic response. The significant enhancement of oxidation peak current at the AuNPs/MMPF-6(Fe)/GCE (14.29 $\mu$A) was about 1.68 times higher than the sum of the peak currents of AuNPs/GCE (2.16 $\mu$A) and MMPF-6(Fe)/GCE (6.34 $\mu$A), indicating the synergistic effect of AuNPs and MMPF-6(Fe).

**Effect of Fe(III) Ions.** To examine the influence of Fe(III) ions for the hydroxylamine oxidation, the cyclic voltammograms of hydroxylamine at AuNPs/MMPF-6/GCE and AuNPs/MMPF-6(Fe)/GCE were investigated. The AuNPs/MMPF-6/GCE exhibits only a small current peak at 0.38 V (Figure 5a). When compared to that at AuNPs/MMPF-6/

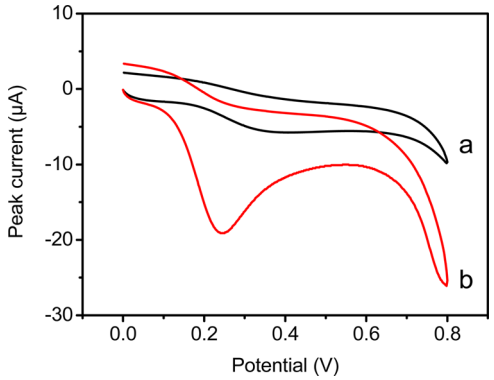


**Figure 5.** Cyclic voltammograms for 0.20 mmol $L^{-1}$ hydroxylamine in 0.1 mol $L^{-1}$ PBS (pH 7.0) at GCEs modified with AuNPs/MMPF-6/GCE (a) and AuNPs/MMPF-6(Fe)/GCE (b) at a scan rate of 100 mV $s^{-1}$.

GCE, the oxidation peak current at AuNPs/MMPF-6(Fe)/GCE increased significantly by about 1.6 times, and the anodic peak potentials are shifted toward negatively of 0.11 V (Figure 5b). The excellent catalytic characteristics of MMPF-6(Fe) could be attributed to the fact that the coordinated metallic ions enhance the conductivity of the MMPF-6, which leads to efficient electron transport through the electrode materials via a tunnelling mechanism.[37,38] Thus, AuNPs/MMPF-6(Fe)/GCE oxidized hydroxylamine at less overpotential with higher current than AuNPs/MMPF-6/GCE.

**Effect of pH.** In general, the value of sample solution pH determines the existing state of hydroxylamine, further affecting their catalytic efficiency. Hydroxylamine is a weakly acidic compound with a p$K_a$ of nearly 5.9, and it exists in both the protonated form of $NH_3OH^+$ and the deprotonated form of $NH_2OH$ depending on the solution pH value. The effect of sample solution pH on the current intensity of hydroxylamine was studied with respect to different pH values (Figure 6). Protonated $NH_3OH^+$ is less electrocatalytic active in comparison with nonprotonated form in the catalytic oxidation process. Hence, the current intensity increased significantly with pH increasing from 5 to 7 and reached the maximum at pH 7.0. Afterward, the peak currents begin to decrease gradually with further increase in pH, which could be attributed to the fact that hydroxylamine will become unstable in high pH values.[7] Hence, pH 7.0 was used in the further experiments. There is a linear relationship between the oxidation peak potential and the solution pH. As shown in the inset of Figure 6, the oxidation peak potential varied linearly with an increasing

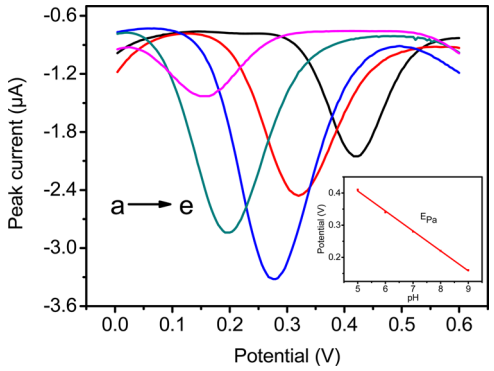


**Figure 6.** Differential pulse voltammograms at AuNPs/MMPF-6(Fe)/GCE modified electrode containing 20.0 $\mu$mol $L^{-1}$ of hydroxylamine 0.1 mol $L^{-1}$ PBS with different pH (a–e: 5.0, 6.0, 7.0, 8.0, and 9.0). Insert: Dependence of oxidation peak potential on solution pH.

pH value, and the regression was $E_{pa}$ (V) = −0.062pH + 0.72 ($R^2$ = 0.9995). The slope of 62 mV $pH^{-1}$ indicates that the number of electrons and protons were the same in the hydroxylamine oxidation reaction.

**Effect of Scan Rate.** The effect of scan rate on the redox reaction of hydroxylamine at the AuNPs/MMPF-6(Fe)/GCE was examined using cyclic voltammetry with scan rate in the range of 10–200 mV $s^{-1}$ and the results were displayed in Figure 7. The anodic peak currents increased gradually and

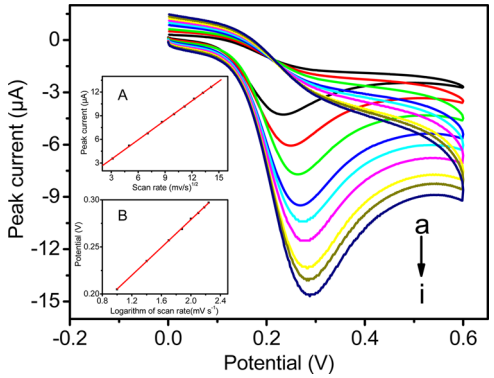


**Figure 7.** Cyclic voltammograms at AuNPs/MMPF-6(Fe)-modified electrode in 0.1 mol $L^{-1}$ PBS (pH 7.0) containing 0.10 mmol $L^{-1}$ of hydroxylamine at different scan rates. (a–i: 10, 25, 50, 75, 100, 125, 150, 175, and 200 mV $s^{-1}$). Insets: (A) Dependence of oxidation peak current on square root of the scan rate. (B) Dependence of peak potentials on logarithm of the scan rate.

linearly with the square root of the scan rates (inset A in Figure 7), and the linear regression equation was $I$ ($\mu$A) = 1.005 + 0.8235$v^{1/2}$ ($mV^{1/2}$ $s^{-1/2}$) ($R^2$ = 0.9999). This indicates that the oxidation of hydroxylamine on AuNPs/MMPF-6(Fe)/GCE is a diffusion-controlled process.

A Tafel plot was drawn to obtain the information in the rate-determining step (inset B of Figure 8). The data can be utilized to estimate the kinetic parameters of electrocatalytic oxidation reaction at the modified electrode surface using following equation.[39]

$$\text{Tafel slope} = (1 - \alpha)n_\alpha F/2.3RT$$

for which $n_\alpha$ is the electron transfer number and $\alpha$ is the electron transfer coefficient. The Tafel slope could be calculated based on slope of $E_{pa}$ with respect to log $v$. In this


DOI: 10.1021/acsami.6b04819
ACS Appl. Mater. Interfaces 2016, 8, 18173–18181

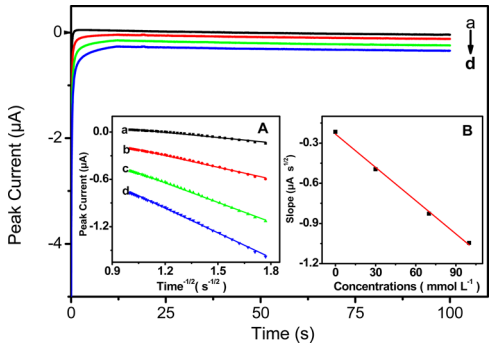


**Figure 8.** Chronoamperometric response at the AuNPs/MMPF-6(Fe)/GCE in 0.1 mol $L^{-1}$ PBS (pH 7.0). Hydroxylamine concentrations: (a) 0, (b) 30.0, (c) 70.0, and (d) 100.0 mmol $L^{-1}$. Insets: (A) Dependence of $I$ on $t^{-1/2}$ derived from chronoamperogram data. (B) Dependence of the slope of straight lines on hydroxylamine concentration.

work, $E_{pa}$ shows a linear relationship with log $v$, and the regression equation can be expressed as $E_{pa}$= 0.0733 log $v$ + 0.1320 ($R^2$ = 0.9997). For a completely irreversible electrode reaction, $\alpha$ is assumed to be 0.6. Then, $n_\alpha$ in the rate-determining step is calculated to be 1.

The total number of electrons ($n$) in the oxidation process at the AuNPs/MMPF-6(Fe)/GCE surface could be calculated based on the Randles−Sevcik equation.[40]

$$I = 3.01 \times 10^5 n[(1-\alpha)n_\alpha]^{1/2} ACD^{1/2}V^{1/2}$$

where $(1-\alpha)n_\alpha$ = 0.4 (as obtained from the above Tafel plots), $A$ is the electrode surface area (0.0314 $cm^2$), $C$ is the bulk concentration of hydroxylamine (mol $cm^{-3}$), and $D$ is the diffusion coefficient (5.88 × $10^{-6}$ $cm^2$ $s^{-1}$, calculated by the following chronoamperometry), respectively. Therefore, the total number of electrons ($n$) involved in the electrode reaction of hydroxylamine is 2, and the oxidation mechanism of hydroxylamine may be expressed in the following reaction:

$$2NH_2OH \rightarrow N_2O + H_2O + 4H^+ + 4e^-$$

**Chronoamperometric Studies.** Generally, the chronoamperometry method was widely used for the determination of diffusion coefficient of target analytes. According to Cottrell's equation in the diffusion control procedure,[39] the current signal can be calculated as follows:

$$I = nFAD^{1/2}C\pi^{-1/2}t^{-1/2}$$

where $C$ is the bulk concentration (mol $cm^{-3}$) and $D$ is the diffusion coefficient ($cm^2$ $s^{-1}$). From inset A of Figure 8, the plot shows the linear dependence between $I$ versus $t^{-1/2}$. The slope was calculated versus the hydroxylamine concentration (inset B of Figure 8); from the value of slope, the diffusion coefficient was calculated to be 5.88 × $10^{-6}$ $cm^2$ $s^{-1}$.

**Effects of Accumulation Potential and Accumulation Time.** With the accumulation potential changed from −0.4 to 0.1 V (Figure 9), the anodic peak current of hydroxylamine increased obviously and then decreased obviously when the accumulation potential changed more positively. Therefore, −0.3 V was used throughout this work. The effect of accumulation time was examined within a range of 60−210 s at a time interval of 30 s. The anodic peak current of hydroxylamine increased achieved the maximum with the accumulation time until 120 s and then kept nearly unchanged at a higher accumulation time. This phenomenon suggested

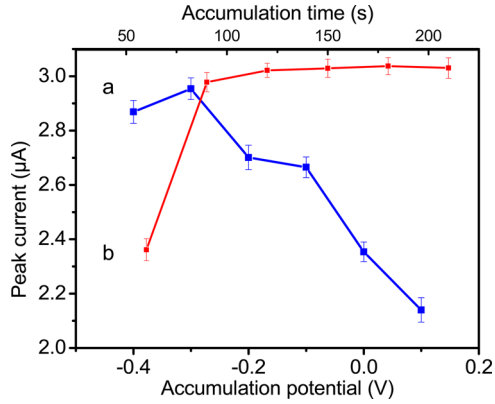


**Figure 9.** Dependence of current intensity of 20 μmol $L^{-1}$ hydroxylamine on accumulation potential (a) and accumulation time (b) in 0.1 mol $L^{-1}$ PBS (pH 7.0).

that the saturated adsorption of hydroxylamine at the electrode surface was achieved. Finally, the accumulation time was adjusted to 120 s as the optimum condition.

**Analytical Performance.** Figure 10 showed the differential pulse voltammograms of hydroxylamine at the AuNPs/MMPF-

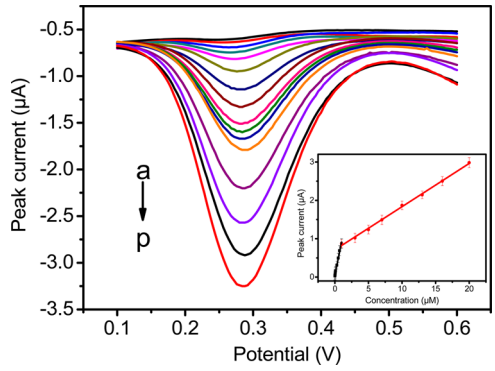


**Figure 10.** Differential pulse voltammograms at AuNPs/MMPF-6(Fe)/GCE for different hydroxylamine concentrations in the pH 7.0 PBS. (a−p: 0.01, 0.03, 0.05, 0.07, 0.1, 0.3, 0.5, 0.7, 1.0, 3.0, 5.0, 7.0, 10, 13, 16, and 20 μmol $L^{-1}$) Inset: calibration curve.

6(Fe)/GCE. Clearly, the anodic oxidation peak currents increased with increasing hydroxylamine concentration within the range of 0.01−20.0 μmol $L^{-1}$. As shown in the inset of Figure 10, two linear ranges were obtained in the ranges of 0.01−1.0 and 1.0−20.0 μmol $L^{-1}$ with the following linear regression: $I_{pa}$ (μA) = 0.8596$C$ (μmol $L^{-1}$) + 0.0518 ($R^2$ = 0.9962) and $I_{pa}$ (μA) = 0.1125$C$ (μmol $L^{-1}$) + 0.7103 ($R^2$ = 0.9992). The first one at lower concentration levels is attributed to an absorption of hydroxylamine on the AuNPs/MMPF-6(Fe)/GCE surface to form a submonolayer; meanwhile, the second one at the higher concentration levels was due to a diffusion process to form a monolayer-covered surface. Comparative studies between the two analytical linear segments revealed that the sensitivity of the second analytical linear segment was lower than that of the first one. This is due to the fact that the mass transfer limitation and the diffusion layer thickness were decreased when hydroxylamine concentration increased in the solution, which resulted in the decrease in the sensitivity of the second analytical linear segment. The detection limit was as low as 0.004 μmol $L^{-1}$ (S/N = 3). The analytical performance of AuNPs/MMPF-6(Fe)-based


DOI: 10.1021/acsami.6b04819
ACS Appl. Mater. Interfaces 2016, 8, 18173−18181

**Table 1. Applications of Electrochemical Methods in the Detection of Hydroxylamine with Different Electrode Materials**

| electrode[a] | methods[b] | linear range ($\mu$M $L^{-1}$) | detection limit ($\mu$M $L^{-1}$) | RSD (%) | ref |
|---|---|---|---|---|---|
| RuON/GCE | DPV | 4.0−78.3 | 0.45 | 5.7 | 14 |
| AuNPs/SWCNT/GCE | amperometry | 16−210 | 0.72 | | 15 |
| BaMWCNT/GCE | amperometry | 0.5−400 | 0.1 | 4.8 | 41 |
| quinizarine/$TiO_2$ nanoparticles/CPE | DPV | 1−400 | 0.173 | | 42 |
| indigocarmine/GCE | DPV | 0.5−18 | 0.16 | | 43 |
| NiHCF/CCE | amperometry | 1.0−50.0 | 0.24 | 2.4 | 44 |
| Ni(II)-MR/MWCNT-PE | amperometry | 2.5−400 | 0.8 | 1.9 | 45 |
| alizarine red S/GCE | amperometry | 10−800 | 7.2 | 4.2 | 46 |
| CGA/MWCNT/GCE | amperometry | 11.8−2900.7 | 1.4 | 4.6 | 47 |
| Co(II)L/MWCNT/CPE | SWV | 5−50 | 1.2 | 3.7 | 48 |
| QMSNPs/GCE | amperometry | 1.0−9410.8 | 0.38 | 2.2 | 49 |
| RMWCNT/GCE | amperometry | 1.0−81.7 | 1.0 | 2.6 | 50 |
| *p*-chloranil/MWCNT/GCE | SWV | 0.1−172.0 | 0.08 | | 51 |
| nano-Pt/Ch/GCE | LSV | 0.5−1900 | 0.07 | 2.8 | 52 |
| HTP/MWCNT/CPE | DPV | 2−8000 | 0.16 | 2.6 | 53 |
| tGO-Pd/GCE | amperometry | 1−10000 | 0.31 | 4.6 | 54 |
| AuNPs/MMPF-6(Fe)/GCE | DPV | 0.01−20 | 0.004 | 2.2 | this work |

[a]RuON: ruthenium oxide nanoparticles; SWCNT: single-walled carbon nanotube; BaMWCNT: baicalin carbon nanotubes; NiHCF: nickel hexacyanoferrate; Ni(II)-MC/MWCNT-PE: nickel(II)-morin complex/multiwall carbon nanotube paste electrode; CGA: chlorogenic acid film; Co(II)L: cobalt(II) bis(benzoylacetone) ethylenediimino; QMSNPs: quinazolin silver nanoparticles; RMWCNT/GCE: rutin multiwall carbon nanotubes; nano-Pt/Ch: Pt nanoclusters on choline film; HTP: 4-hydroxy-2-(triphenylphosphonio) phenolate; DMPP: 2,2′-(4,5-dihydroxy-3-methoxy-1,2-phenylene) bis(3-oxo-3-phenyl propanenitrile); tGO-Pd: Pd nanoparticle catalysts supported by thiolated graphene oxide. [b]DPV: differential pulse voltammetry; SWV: square wave voltammetry.

**Table 2. Comparison of the Proposed Sensor with Other Reported Methods for the Determination of Hydroxylamine**

| methods | linear range ($\mu$mol $L^{-1}$) | detection limit ($\mu$mol $L^{-1}$) | RSD (%) | ref |
|---|---|---|---|---|
| gas chromatograph | 0.14−3.57 | | | 7 |
| flow-injection biamperometry | 0.6−40 | 0.1 | 1.4 | 55 |
| gas chromatograph | | 0.045 | 5.0 | 56 |
| spectrophotometric method | 0−0.21 | | 1.2 | 57 |
| chemiluminescence | 0.08−2 | 0.04 | 2.0 | 58 |
| indirect kinetic spectrophotometry | 0.001−0.036 | 0.0003 | 1.18 | 59 |
| differential pulse polarography | 2−2000 | 1 | <8.0 | 60 |
| AuNPs/MMPF-6(Fe)/GCE | 0.01−20 | 0.004 | 2.2 | this work |

electrochemical sensor was compared with other electrode materials.[14,15,41−54] From Table 1, it is obvious that the fabricated electrode had the lowest detection limit and two wider linear regions, suggesting that the fabricated AuNPs/MMPF-6(Fe)-based sensor was superior. At the same time, a comparison of the other reported methods for hydroxylamine detection with the proposed electrochemical sensor was also made, and the results are presented in Table 2.[7,55−60]

The AuNPs/MMPF-6(Fe)-modified electrode showed good reproducibility for hydroxylamine detection. The relative standard deviation of 10 $\mu$mol $L^{-1}$ hydroxylamine was 2.2% ($n$ = 10). In addition, seven electrodes prepared with the same procedure were investigated in 10 $\mu$mol $L^{-1}$ hydroxylamine, and a relative standard deviation of 4.3% was obtained. Generally, most bare MOFs-based electrode material is unstable in acidic media, which could be destroyed in the subsequent potential scan cycles. The stability of AuNPs/MMPF-6(Fe) was checked by recording 100 successive adsorptive/stripping cycles in 0.1 mol $L^{-1}$ supporting electrolyte with 10 $\mu$mol $L^{-1}$ hydroxylamine, and the electrode still possessed more than 85% current intensity. The exceptional stability of MMPF-6(Fe) could be due to the stable building units of Zr6 cluster in the MOF structure as well as the coordinate effect between the porphyrin macrocyclic ring and Fe(III). Therefore, the whole framework materials demonstrated high resistance to the acid solution, indicating that AuNPs/MMPF-6(Fe)/GCE possess extraordinary stability and has a great potential in practical of reuse.

**Sample Analysis and Interference Studies.** The practical application of the fabricated AuNPs/MMPF-6(Fe)/GCE was used to direct analysis hydroxylamine in oxyurea capsule, PAM injection, and water samples. As shown in Table 3, recoveries between 95.4 and 103.0% are acceptable. Thus, the established approach could be used to the determination of hydroxylamine levels in real samples.

In environmental and biological samples, hydroxylamine could suffer from the potential interferences in their analysis. Thus, experiment with potentially interfering substances was carried out to study the selectivity of AuNPs/MMPF-6(Fe)-modified electrode. The tolerable concentration was defined as the current deviations caused by interference not exceeding ±5.0%. The results suggested that 100-fold concentration of $N_2H_4$, 500-fold concentration of $Ca^{2+}$ (3.5%), $Ba^{2+}$ (3.1%), $Pb^{2+}$ (4.6%), $Cd^{2+}$ (4.1%), $Cu^{2+}$ (4.3%), $Co^{2+}$ (3.9%), and $Mn^{2+}$ (4.1%), and 1000-fold concentration of $K^+$ (4.5%), $Na^+$ (4.1%), $PO_4^{3-}$ (4.3%), $HPO_4^{2-}$ (4.6%), $H_2PO^{4-}$ (4.3%), $NH_4^+$ (4.4%), $SO_4^{2-}$ (4.5%), and $Cl^-$ (4.1%) have no influence on the current intensity of 10.0 $\mu$mol $L^{-1}$ hydroxylamine. In addition, dopamine (4.6%), glucose (4.5%), fructose (4.5%), lactose (4.6%), and sucrose (4.1%) showed no obvious changes in the


DOI: 10.1021/acsami.6b04819
ACS Appl. Mater. Interfaces 2016, 8, 18173−18181

**Table 3. Determination of Hydroxylamine in Pharmaceutical and Water Samples**

| sample | add ($\mu$mol $L^{-1}$) | found ($\mu$mol $L^{-1}$) | recovery (%) | RSD (%) |
|---|---|---|---|---|
| | 0.00 | 5.20 ± 0.03 | | 2.5 |
| oxyurea capsule | 5.00 | 9.97 ± 0.02 | 95.4 | 1.7 |
| | 10.00 | 15.41 ± 0.04 | 102.1 | 2.2 |
| | 0.00 | 0.25 ± 0.08 | | 2.8 |
| PAM injection | 0.50 | 0.74 ± 0.05 | 98.0 | 2.4 |
| | 1.00 | 1.26 ± 0.06 | 101.0 | 1.6 |
| | 0.00 | | | |
| tap water | 1.00 | 1.02 ± 0.03 | 102.0 | 2.9 |
| | 2.00 | 2.01 ± 0.02 | 100.5 | 2.4 |
| | 0.00 | | | |
| river water | 1.00 | 1.03 ± 0.4 | 103.0 | 3.1 |
| | 2.00 | 2.05 ± 0.03 | 102.5 | 2.8 |

current intensity until a 200-fold excess was used. More importantly, some nitrogen compounds such as ammonia, nitrite, nitrate, and hydrazine are electroactive and usually present in various industrial processes. The results show that 400-fold concentration of $NO_3^-$ (4.5%) and $NO_2^-$ (4.7%), 50-fold concentration of $NH_3^+$ (4.1%), and 50-fold concentration of hydrazine (4.3%) have no interference on 10.0 $\mu$mol $L^{-1}$ hydroxylamine determination. The above results showed that the most common interfering species have no impact on the AuNPs/MMPF-6(Fe)/GCE in the detection of hydroxylamine in water and pharmaceutical samples.

## CONCLUSIONS

AuNPs/MMPF-6(Fe) composites were synthesized and utilized as novel electrode material for the detection of hydroxylamine. The sensor could lower the anodic over potentials and significantly increase the anodic peak currents due to the synergistic effects from the excellent electrical conductivity of AuNPs and the catalytic effect of MMPF-6(Fe). The stable and reproducible sensing layer leads to a considerable improvement in reproducibility and anti-interference ability in the sample analysis. More importantly, the sensor showed a significantly lower detection limit up to nanomolar levels and a wider linear range. These attractive analytical performances made this composites electrode promising in biochemical determination for practical purposes.

## AUTHOR INFORMATION

### Corresponding Authors

*E-mail: wangyzu@126.com.

*E-mail: sqma@usf.edu.

### Notes

The authors declare no competing financial interest.

## ACKNOWLEDGMENTS

This work was supported by the National Natural Science Foundation of China (21205103), the Key Laboratory Foundation of Environmental Material and Engineering of Jiangsu Province (K13077, K14020), and a Project Funded by the Priority Academic Program Development of Jiangsu Higher Education Institutions. Partial support from the University of South Florida and NSF (DMR-1352065) is also acknowledged (S.M.).

## REFERENCES

(1) Leroux, A.; Junien, C.; Kaplan, J. C.; Bamberger, J. Generalised Deficiency of Cytochrome $b_5$ Reductase in Congenital Methaemoglobinaemia with Mental Retardation. *Nature* **1975**, *258*, 619−620.

(2) Choudhary, G.; Hansen, H. Human Health Perspective of Environmental Exposure to Hydrazines: A Review. *Chemosphere* **1998**, *37*, 801−843.

(3) Smith, R. P.; Layne, W. R. A Comparison of the Lethal Effects of Nitrite and Hydroxylamine in the Mouse. *J. Pharmacol. Exp. Ther.* **1969**, *165*, 30−35.

(4) Gross, P.; Smith, R. P. Biologic Activity of Hydroxylamine: a Review. *CRC Crit. Rev. Toxicol* **1985**, *14*, 87−99.

(5) Fiadeiro, M.; Solorzano, L.; Strickland, J. D. H. Hydroxylamine in Seawater. *Limnol. Oceanogr.* **1967**, *12*, 555−556.

(6) Anderson, J. H. The Copper-catalysed Oxidation of Hydroxylamine. *Analyst* **1964**, *89*, 357−362.

(7) Seike, Y.; Fukumori, R.; Senga, Y.; Oka, H.; Fujinaga, K.; Okumura, M. A Simple Sensitive Method for the Determination of Hydroxylamine in Fresh-Water Sanples Using Hypochlorite Followed by Gas Chromatography. *Anal. Sci.* **2004**, *20*, 139−142.

(8) Zhang, C.; Wang, G.; Liu, M.; Feng, Y.; Zhang, Z.; Fang, B. A Hydroxylamine Electrochemical Sensor Based on Eectrodeposition of Porous ZnO Nanofilms onto Carbon Nanotubes Films Modified Electrode. *Electrochim. Acta* **2010**, *55*, 2835−2840.

(9) Moghaddam, H. M.; Beitollahi, H.; Tajik, S.; Malakootian, M.; Maleh, H. K. Simultaneous Determination of Hydroxylamine and Phenol Using a Nanostructure-based Electrochemical Sensor. *Environ. Monit. Assess.* **2014**, *186*, 7431−7441.

(10) Safavi, A.; Shojaeifard, Z.; Tohidi, M. Fabrication of an Amperometric Sensor for Hydroxylamine Based on Silver Paste Nanocomposite Electrode. *IEEE Sens. J.* **2014**, *14*, 839−846.

(11) Foroughi, M. M.; Beitollahi, H.; Tajik, S.; Hamzavi, M.; Parvan, H. Hydroxylamine Electrochemical Sensor Based on a Modified Carbon Nanotube Paste Electrode: Application to Determination of Hydroxylamine in Water Samples. *Int. J. Electrochem. Sci.* **2014**, *9*, 2955−2965.

(12) Benvidi, A.; Jahanbani, S.; Akbari, A.; Zare, H. R. Simultaneous Determination of Hydrazine and Hydroxylamine on a Magnetic Bar Carbon Paste Electrode Modified with Reduced Graphene Oxide/$Fe_3O_4$ Nanoparticles and a Heterogeneous Mediator. *J. Electroanal. Chem.* **2015**, *758*, 68−77.

(13) Li, J.; Lin, X. Electrocatalytic Oxidation of Hydrazine and Hydroxylamine at Gold Nanoparticle-Polypyrrole Nanowire Modified Glassy Carbon Electrode. *Sens. Actuators, B* **2007**, *126*, 527−535.

(14) Zare, H. R.; Hashemi, S. H.; Benvidi, A. Electrodeposited Nanoscale Islands of Ruthenium Oxide as a Bifunctional Electrocatalyst for Simultaneous Catalytic Oxidation of Hydrazine and Hydroxylamine. *Anal. Chim. Acta* **2010**, *668*, 182−187.

(15) Bui, M. P. N.; Pham, X. H.; Han, K. N.; Li, C. A.; Lee, E. K.; Chang, H. J.; Seong, G. H. Electrochemical Sensing of Hydroxylamine by Gold Nanoparticles on Single-walled Carbon Nanotube Films. *Electrochem. Commun.* **2010**, *12*, 250−253.

(16) Férey, G.; Mellot Draznieks, C.; Serre, C.; Millange, F. Crystallized Frameworks with Giant Pores: Are There Limits to the Possible? *Acc. Chem. Res.* **2005**, *38*, 217−225.

(17) Yaghi, O. M.; O'Keeffe, M.; Ockwig, N. W.; Chae, H. K.; Eddaoudi, M.; Kim, J. Reticular Synthesis and the Design of New Materials. *Nature* **2003**, *423*, 705−714.

(18) Jeong, N. C.; Samanta, B.; Lee, C. Y.; Farha, O. K.; Hupp, J. T. Coordination-chemistry Control of Proton Conductivity in the Iconic Metal-organic Framework Material HKUST-1. *J. Am. Chem. Soc.* **2012**, *134*, 51−54.

(19) Rowsell, J. L. C.; Yaghi, O. M. Effects of Functionalization, Catenation, and Variation of the Metal Oxide and Organic Linking Units on the Low-Pressure Hydrogen Adsorption Properties of Metal-Organic Frameworks. *J. Am. Chem. Soc.* **2006**, *128*, 1304−1315.

(20) Schlichte, K.; Kratzke, T.; Kaskel, S. Improved Synthesis, Thermal Stability and Catalytic Properties of the Metal-organic



DOI: 10.1021/acsami.6b04819
*ACS Appl. Mater. Interfaces* 2016, 8, 18173−18181

Framework Compound $Cu_3(BTC)_2$. *Microporous Mesoporous Mater.* **2004**, *73*, 81−88.
(21) Hosseini, H.; Ahmar, H.; Dehghani, A.; Bagheri, A.; Tadjarodi, A.; Fakhari, A. R. A Novel Electrochemical Sensor Based on Metal-organic Framework for Electro-catalytic Oxidation of L-cysteine. *Biosens. Bioelectron.* **2013**, *42*, 426−429.
(22) (a) Kung, C. W.; Chang, T. H.; Chou, L. Y.; Hupp, J. T.; Farha, O. K.; Ho, K. C. Porphyrin-based Metal-organic Framework Thin Films for Electrochemical Nitrite Detection. *Electrochem. Commun.* **2015**, *58*, 51−56.
(23) Fernandes, D. M.; Barbosa, A. D.; Pires, J.; Balula, S. S.; Cunha Silva, L.; Freire, C. Novel Composite Material Polyoxovanadate@MIL-101(Cr): A Highly Efficient Electrocatalyst for Ascorbic Acid Oxidation. *ACS Appl. Mater. Interfaces* **2013**, *5*, 13382−13390.
(24) Zhang, Y. F.; Bo, X. J.; Luhana, C.; Wang, H.; Li, M.; Guo, L. P. Facile Synthesis of A Cu-based MOF Confined in Macroporous Carbon Hybrid Material with Enhanced Electrocatalytic Ability. *Chem. Commun.* **2013**, *49*, 6885−6887.
(25) Wang, X.; Wang, Q.; Wang, Q.; Gao, F.; Gao, F.; Yang, Y.; Guo, H. Highly Dispersible and Stable Copper Terephthalate Metal-organic Framework-graphene Oxide Nanocomposite for An Electrochemical Sensing Application. *ACS Appl. Mater. Interfaces* **2014**, *6*, 11573−11580.
(26) Daniel, M. C.; Astruc, D. Gold Nanoparticles: Assembly, Supramolecular Chemistry, Quantum-Size-Related Properties, and Applications toward Biology, Catalysis, and Nanotechnology. *Chem. Rev.* **2004**, *104*, 293−346.
(27) Afkhami, A.; Soltani Felehgari, F.; Madrakian, T.; Ghaedi, H. Surface Decoration of Multi-walled Carbon Nanotubes Modified Carbon Paste Electrode with Gold Nanoparticles for Electro-oxidation and Sensitive Determination of Nitrite. *Biosens. Bioelectron.* **2014**, *51*, 379−385.
(28) Liu, H.; Liu, Y.; Li, Y.; Tang, Z.; Jiang, H. Metal-Organic Framework Supported Gold Nanoparticles as a Highly Active Heterogeneous Catalyst for Aerobic Oxidation of Alcohols. *J. Phys. Chem. C* **2010**, *114*, 13362−13369.
(29) Jiang, H. L.; Liu, B.; Akita, T.; Haruta, M.; Sakurai, H.; Xu, Q. Au@ZIF-8: CO Oxidation over Gold Nanoparticles Deposited to Metal-Organic Framework. *J. Am. Chem. Soc.* **2009**, *131*, 11302−11303.
(30) Wu, R.; Qian, X.; Zhou, K.; Liu, H.; Yadian, B.; Wei, J.; Zhu, H.; Huang, Y. Highly Dispersed Au Nanoparticles Immobilized on Zr-based Metal-organic Frameworks as Heterostructured Catalyst for CO Oxidation. *J. Mater. Chem. A* **2013**, *1*, 14294−14299.
(31) Ke, F.; Zhu, J.; Qiu, L. G.; Jiang, X. Controlled Synthesis of Novel Au@MIL-100(Fe) Core-shell Nanoparticles with Enhanced Catalytic Performance. *Chem. Commun.* **2013**, *49*, 1267−1269.
(32) Chen, Y.; Hoang, T.; Ma, S. Biomimetic Catalysis of a Porous Iron-Based Metal-Metalloporphyrin Framework. *Inorg. Chem.* **2012**, *51*, 12600−12602.
(33) Feng, D.; Gu, Z. Y.; Li, J. R.; Jiang, H. L.; Wei, Z.; Zhou, H. C. Zirconium-metalloporphyrin PCN-222: Mesoporous Metal-organic Frameworks with Ultrahigh Stability as Biomimetic Catalysts. *Angew. Chem., Int. Ed.* **2012**, *51*, 10307−10310.
(34) Morris, W.; Volosskiy, B.; Demir, S.; Gandara, F.; McGrier, P. L.; Furukawa, H.; Cascio, D.; Stoddart, J. F.; Yaghi, O. M. Synthesis, Structure, and Metalation of two new Highly Porous Zirconium Metal-organic Frameworks. *Inorg. Chem.* **2012**, *51*, 6443−6445.
(35) Frens, G. Controlled Nucleation for the Regulation of the Partical Size in Monodisperse Gold Suspensions. *Nature, Phys. Sci.* **1973**, *241*, 20−22.
(36) Zhao, H.; Chang, Y.; Liu, C. Electrodes Modified with Iron Porphyrin and Carbon Nanotubes: Application to $CO_2$ Reduction and Mechanism of Synergistic Electrocatalysis. *J. Solid State Electrochem.* **2013**, *17*, 1657−1664.
(37) Zhang, X. Q.; Wu, H. M.; Wei, Y.; Cheng, Z. P.; Wu, X. J. Structure and Conductivity Anisotropy of a New Porphyrin Langmuir-Blodgett Film. *Solid State Commun.* **1995**, *95*, 99−101.
(38) Lu, X.; Li, M.; Yang, C.; Zhang, L.; Li, Y.; Jiang, L.; Li, H.; Jiang, L.; Liu, C.; Hu, W. Electron Transport through a Self-Assembled Monolayer of Thiol-End-Functionalized Tetraphenylporphines and Metal Tetraphenylporphines. *Langmuir* **2006**, *22*, 3035−3039.
(39) Bard, A. J.; Faulkner, L. R. *Electrochemical Methods: Fundamentals and Applications*; Wiley: New York, 1980; pp 121−122.
(40) Antoniadou, S.; Jannakoudakis, A. D.; Theodoridou, E. Electrocatalytic Reactions on Carbon Fibre Electrodes Modified by Hemine II. Electro-oxidation of Hydrazine. *Synth. Met.* **1989**, *30*, 295−304.
(41) Zhang, H.; Zheng, J. Sensitive Detection of Hydroxylamine at a Simple Baicalin Carbon Nanotubes Modified Electrode. *Talanta* **2012**, *93*, 67−71.
(42) Mazloum Ardakani, M.; Beitollahi, H.; Taleat, Z.; Naeimi, H. Voltammetric Determination of Hydroxylamine at the Surface of a Quinizarine/$TiO_2$ Nanoparticles-modified Carbon Paste Electrode. *Anal. Methods* **2010**, *2*, 1764−1769.
(43) Mazloum Ardakani, M.; Taleat, Z. Investigation of Electrochemistry Behavior of Hydroxyl-amine at Glassy Carbon Electrode by Indigocarmine. *Int. J. Electrochem. Sci.* **2009**, *4*, 694−706.
(44) Salimi, A.; Abdi, K. Enhancement of the Analytical Properties and Catalytic Activity of a Nickel Hexacyanoferrate Modified Carbon Ceramic Electrode Prepared by Two-step Sol-gel Technique: Application to Amperometric Detection of Hydrazine and Hydroxyl Amine. *Talanta* **2004**, *63*, 475−483.
(45) Zheng, L.; Song, J. F. Electrocatalytic Oxidation of Hydroxylamine at Ni(II)-morin Complex Modified Carbon Nanotube Paste Electrode. *J. Appl. Electrochem.* **2011**, *41*, 63−70.
(46) Ardakani, M. M.; Karimi, M. A.; Mirdehghan, S. M.; Zare, M. M.; Mazidi, R. Electrocatalytic Determination of Hydroxylamine with Alizarin Red S as a Homogenous Mediator on the Glassy Carbon Electrode. *Sens. Actuators, B* **2008**, *132*, 52−59.
(47) Zare, H. R.; Nasirizadeh, N.; Ajamain, H.; Sahragard, A. Preparation, Electrochemical Behavior and Electrocatalytic Activity of Chlorogenic Acid Multi-wall Carbon Nanotubes as a Hydroxylamine Sensor. *Mater. Sci. Eng., C* **2011**, *31*, 975−982.
(48) Benvidi, A.; Kakoolaki, P.; Gorji, A. R.; Mazloum Ardakani, M.; Zare, H. R.; Vafazadeh, R. Application of Co(ii) Complex Multi-wall Carbon Nanotube Modified Carbon Paste Electrodes for Electrocatalytic Determination of Hydroxylamine. *Anal. Methods* **2013**, *5*, 6649−6655.
(49) Nasirizadeh, N.; Aghayizadeh, M. M.; Bidoki, S. M.; Yazdanshenas, M. E. A Novel Sensor of Quinazolin Derivative Self-Assembled Monolayers over Silver Nanoparticles for the Determination of Hydroxylamine. *Int. J. Electrochem. Sci.* **2013**, *8*, 11264−11277.
(50) Zare, H. R.; Sobhani, Z.; Mazloum Ardakani, M. Electrocatalytic Oxidation of Hydroxylamine at a Rutin Multi-wall Carbon Nanotubes Modified Glassy Carbon Electrode: Improvement of the Catalytic Activity. *Sens. Actuators, B* **2007**, *126*, 641−647.
(51) Sadeghi, R.; Karimi Maleh, H.; Khalilzadeh, M. A.; Beitollahi, H.; Ranjbarha, Z.; Zanousi, M. B. A New Strategy for Determination of Hydroxylamine and Phenol in Water and Waste Water Samples Using Modified Nanosensor. *Environ. Sci. Pollut. Res.* **2013**, *20*, 6584−6593.
(52) Li, J.; Xie, H. A Hydroxylamine Electrochemical Sensor based on Electrodeposition of Platinum Nanoclusters on Choline Film Modified Glassy Carbon Electrode. *J. Appl. Electrochem.* **2012**, *42*, 271−277.
(53) Shishehbore, M. R.; Zare, H. R.; Nematollahi, D.; Saber-Tehrani, M. Electrocatalytic Oxidation and Differential Pulse Voltammetric Determination of Hydroxylamine Using a 4-hydroxy-2-(triphenylphosphonio)phenolatecarbon Nanotubes Modified Electrode. *Anal. Methods* **2011**, *3*, 306−313.
(54) Lee, E.; Kim, D.; You, J. M.; Kim, S. K.; Yun, M.; Jeon, S. Electrocatalytic Oxidation of Hydrazine and Hydroxylamine by Graphene Oxide-Pd Nanoparticle-Modified Glassy Carbon Electrode. *J. Nanosci. Nanotechnol.* **2012**, *12*, 8886−8892.


DOI: 10.1021/acsami.6b04819
*ACS Appl. Mater. Interfaces* 2016, 8, 18173−18181

(55) Zhao, C.; Song, J. Flow-Injection Biamperometry for Direct Determination of Hydroxylamine at Two Pretreated Platinum Electrodes. *Anal. Chim. Acta* **2001**, *434*, 261−267.
(56) Guzowski, J. P.; Golanoski, C.; Montgomery, E. R. A Gas Chromatographic Method for the Indirect Determination of Hydroxylamine in Pharmaceutical Preparations: Conversion into Nitrous Oxide. *J. Pharm. Biomed. Anal.* **2003**, *33*, 963−974.
(57) Deepa, B.; Balasubramanian, N.; Nagaraja, K. S. Spectrophotometric Determination of Hydroxylamine and Its Derivatives in Pharmaceuticals. *Chem. Pharm. Bull.* **2004**, *52*, 1473−1475.
(58) Zhang, S. C.; Zhou, G. J.; Ju, H. X. Chemiluminescence Sensor for the Determination of Hydroxylamine by Electrostatically Immobilizing Luminol and Periodate. *Chem. Res. Chinese U.* **2003**, *19*, 155−159.
(59) Afkhami, A.; Madrakian, T.; Maleki, A. Indirect Kinetic Spectrophotometric Determination of Hydroxylamine Based on Its Reaction with Iodate. *Anal. Sci.* **2006**, *22*, 329−331.
(60) Combeau, S.; Legeai, S.; Chatelut, M.; Vittori, O.; Devisme, F. Simultaneous Determination of Hydrogen Peroxide, Hydroxylamine and Iodate in Basic Media by Differential Pulse Polarography. *J. Nucl. Sci. Technol.* **2005**, *42*, 82−89.



DOI: 10.1021/acsami.6b04819
*ACS Appl. Mater. Interfaces* 2016, 8, 18173−18181